Supplemental Material for Left atrial appendage electrical isolation reduces atrial fibrillation recurrences: a simulation study

Ali Gharaviri, PhD; Simone Pezzuto, PhD; Mark Potse, PhD; Sander Verheule, PhD, Giulio Conte, MD, PhD, Rolf Krause, PhD, Ulrich Schotten, MD, PhD, and Angelo Auricchio, MD, PhD.

S1 Computational model of AF

A structurally detailed model of the human atria, extensively described previously[1], was used in this study. The global geometry was reconstructed using magnetic resonance image data of a subject with normal atria. Additional anatomical structures and properties, such as wall thickness heterogeneities, twenty pectinate muscles, Bachmann's Bundle, interatrial bundles, and the crista terminalis, and left atrial appendage trabeculated network were added manually.[2] One to three layers of fiber orientations manually included in the model based on anatomical studies using a combination of manual editing and computer algorithms.[1] These structures are considered to play a key role in AF initiation and maintenance. [3, 4]

Simulations were performed with a second-order accurate finite-difference method [5] on a hexahedral mesh at 0.2mm resolution including of approximately 5 million nodes. Differential equations for potentials and ion concentrations were integrated with the forward Euler method and gating variables with the Rush-Larsen method[6] using a time step of 0.01ms. The implementation of the boundary conditions is implicit in the formulation of Saleheen and Ng.[7]. Simulations were performed with a monodomain reaction-diffusion model using the propag-5 software[8] and run on a Cray XC50 supercomputer with GPU support.

The material properties for the atria were set to produce an approximately normal P wave in case of sinus rhythm.[2] The effective monodomain conductivities along and across the fiber

are given in Table S1. The tissue surface to volume ratio was 800 cm^{-1} throughout the atrial myocardium.

Ionic currents for each node were described by the Courtemanche-Ramirez-Nattel model.[9] Changes in ionic currents caused by AF were incorporated by setting the conductivities for I_{to}, $I_{Ca,L}$, and I_{K1} at 40%, 35%, and 200% of their normal values, respectively.[10]

S2 Fibrosis distribution

Fibrosis patterns similar to those obtained from LGE-MRI were generated with an algorithm that produces spatially-correlated, anatomy-tailored random fields (Figure S1).[1, 11]

The fibrosis was distributed within the atrial wall, while the endocardial bundles remain intact. The spatial distribution of fibrosis was uneven, with patches or island presenting higher degree of fibrosis. Such distribution was based on spatially correlated, anatomy-tailored random fields (Figure S1).[1, 11, 12] Fibrotic elements were assumed to be electrically active and conductive along the fiber direction and electrically isolated in the transverse direction (Table S1). The fibrosis was modelled in this way to represent the loss of side-to-side electrical connections between atrial muscle bundles found by Spach et al. in fibrotic atrial tissue.[13] Simulations were performed without fibrosis, with moderate fibrosis, and with severe fibrosis, in which 0%, 50%, and 70% of elements were fibrotic as described earlier. [1]

S3 AF initiation in pre- and post-catheter ablations

In order to assess the likelihood of AF initiation, both before and after catheter ablations, 20 pacing locations were selected in both atria, including the area between the PVs, left atrium (LA), left atrial appendage (LAA), right atrial appendage (RAA), coronary sinus, superior caval vein (SCV), inferior caval vein (ICV), and right atrium (RA). These points were selected based on reported possible sources of extra-PV ectopic focal activity in AF

patients.[14] All pacing points, except the one located on the LAA were located outside the ablated area. As a consequence, in simulations with LAAI the AF initiation rates were corrected by excluding simulations in which pacing point was located in the LAA. In each simulation one pacing point were selected. The stimulation protocol consisted of a 2 seconds incremental pacing from a selected location, in which a train of stimuli with progressive reduction in pacing interval was applied, followed by 3 seconds of simulation with no pacing.

S4 Definition of a successful AF initiation

The outcome of the stimulation protocol was analyzed in terms of the type of self-sustained rhythm after 2 seconds of stimulations. In the presence of no activity, the initiation was considered unsuccessful. Otherwise, a distinction between AF and atrial flutter (AFL) was made, with the latter not being considered a successful AF initiation. To differentiate between AF and AFL conduction patterns, we computed 12-leads ECGs from the simulated atrial electrical activity. To construct the ECGs, the atrial model was incorporated into an inhomogeneous torso model including lungs and intracavitary blood masses. Body surface potentials were simulated using a bi-domain equation solved at 1-mm resolution.[2]

In all 12-lead ECGs, after the pacing periods, we detected positive fibrillation wave peaks and calculated fibrillation cycle length (FCL) as the time interval between two successive F-wave peaks (Figure S2-A). These FCL lengths were used to generate Poincaré plots (Figure S2-B &C). The FCL were described as a vector $FCL = [l_1, l_2, \dots, l_N]$, where l_i is the *i*th FCL. Each Poincaré plot is composed of the points of l_i on the x-axis versus l_{i+1} on the y-axis. The point cloud dispersion (PCD) in Poincaré plots was used as a sensitive parameter describing the regularity of activations and to differentiate between AFL and AF simulations. PCD were calculated using as an averaged Euclidean distance of each point in a point cloud to the point cloud centroid:

$$PCD = \frac{1}{N-1}\sum_{i=1}^{N-1}\sqrt{(l_i - c_x)^2 + (l_{i+1} - c_y)^2} \quad (1)$$

where $C(c_x, c_y)$ is the centroid of the point cloud in Poincaré plot. Finally, by applying an arbitrary threshold to the PCD we classified AF conduction patterns in simulations from AFL. All algorithms were developed in Matlab (v. R2016a, Mathworks).

Figure S3 illustrates representative conduction patterns of simulations and corresponding three-lead ECG in the control group with three different degrees of fibrosis. In the absence of fibrosis AF was not inducible while in moderate and severe fibrosis the stimulation of the atria resulted in AF induction. Figure S4 shows activation patterns in PVI + LAAI simulations and corresponding ECGs without fibrosis, with moderate fibrosis, and with severe fibrosis. In these examples, AF was inducible only in severe fibrosis but not without or in moderate fibrosis.

S5 Detection and tracking fibrillation waves

A fibrillation wave was defined as a contiguous volume in which all nodes had transmembrane voltages above −60mV. The number of waves was calculated at each millisecond of simulated time.

Fibrillation waves were tracked in both time and space, as described in our previous study.[15] Briefly, the temporal dynamics of waves can be described by three events:

- Generation: appearance of a new wave due to a wave breaking up into two or more waves.
- Fusion: the fusion of two or more waves into one wave as they merge with each other.
- Extinction: the extinction of a wave, because either it hits a boundary or runs into unexcitable tissue.

S6 Statistics

All statistical analyses were performed using GraphPad Prism software version 8.0. All values were expressed as the mean ± SD. Statistical tests were performed to compare the effect of two parameters, fibrosis levels and ablation patterns, in AF initiation rate, using Two-Way ANOVA followed by post hoc Bonferroni test. A value of $P < 0.05$ was considered significant.

Figure legends:

Figure S1: Posterior and anterior view of the atria with patchy fibrosis. A) Patchy fibrosis model, 50% fibrotic (anterior view). B) Patchy fibrosis model, 50% fibrotic (posterior view). C) Cross sectional view of the atrial geometry demonstrating fibrosis distribution within the atrial wall.

Figure S2: Local electrograms recorded during simulated AF episodes at 4 different point on both atria (E1-E4) and 2 ECG leads (II and V1).

Figure S3: Atrial tachycardia patterns. A) An example of simulated lead II ECG in a simulation with atrial fibrillation conduction pattern. Red stars indicate the positive peak of the fibrillation wave. B) Corresponding Poincaré plot generated from the ECG presented in section A. C) An example of ECGs (Lead I, II, and V1) and corresponding Poincaré plots in a simulation with flutter conduction pattern. D) An example of ECGs and corresponding Poincaré plots in a simulation with a fibrillation conduction pattern.

Figure S4: AF initiation in control simulations. A) Consecutive snapshots of conduction patterns and corresponding three ECG leads (II, V1, and V3) in control simulations with no, moderate, and severe fibrotic simulations.

Figure S5: AF initiation in ablation simulations. Series of conduction pattern snapshots in simulations with pulmonary vein isolations accompanied by LAA isolation and their corresponding three ECG leads (II, V1, and V3) without, with moderate, and with severe fibrosis.

References:

1. Gharaviri A, Bidar E, Potse M, Zeemering S, Verheule S, Pezzuto S, Krause R, Maessen JG, Auricchio A and Schotten U. Epicardial Fibrosis Explains Increased Endo-Epicardial Dissociation and Epicardial Breakthroughs in Human Atrial Fibrillation. *Front Physiol*. 2020;11:68.
2. Potse M, Lankveld TA, Zeemering S, Dagnelie PC, Stehouwer CD, Henry RM, Linnenbank AC, Kuijpers NH and Schotten U. P-wave complexity in normal subjects and computer models. *J Electrocardiol*. 2016;49:545-53.
3. Whitaker J, Rajani R, Chubb H, Gabrawi M, Varela M, Wright M, Niederer S and O'Neill MD. The role of myocardial wall thickness in atrial arrhythmogenesis. *Europace*. 2016;18:1758-1772.
4. Verheule S, Eckstein J, Linz D, Maesen B, Bidar E, Gharaviri A and Schotten U. Role of endo-epicardial dissociation of electrical activity and transmural conduction in the development of persistent atrial fibrillation. *Prog Biophys Mol Biol*. 2014;115:173-85.
5. Potse M, Dube B, Richer J, Vinet A and Gulrajani RM. A comparison of monodomain and bidomain reaction-diffusion models for action potential propagation in the human heart. *IEEE Trans Biomed Eng*. 2006;53:2425-35.
6. Rush S and Larsen H. A practical algorithm for solving dynamic membrane equations. *IEEE Trans Biomed Eng*. 1978;25:389-92.
7. Saleheen HI and Ng KT. New finite difference formulations for general inhomogeneous anisotropic bioelectric problems. *IEEE Trans Biomed Eng*. 1997;44:800-9.
8. Krause D, Potse M, Dickopf T, Krause R, Auricchio A and Prinzen F. Hybrid Parallelization of a Large-Scale Heart Model. In: R. Keller, D. Kramer and J.-P. Weiss, eds. *Facing the Multicore - Challenge II*: Springer Berlin Heidelberg; 2012(7174): 120-132.
9. Courtemanche M, Ramirez RJ and Nattel S. Ionic mechanisms underlying human atrial action potential properties: insights from a mathematical model. *Am J Physiol*. 1998;275:H301-21.
10. Gharaviri A, Verheule S, Eckstein J, Potse M, Kuklik P, Kuijpers NH and Schotten U. How disruption of endo-epicardial electrical connections enhances endo-epicardial conduction during atrial fibrillation. *Europace*. 2017;19:308-318.
11. Pezzuto S, Gharaviri A, Schotten U, Potse M, Conte G, Caputo ML, Regoli F, Krause R and Auricchio A. Beat-to-beat P-wave morphological variability in patients with paroxysmal atrial fibrillation: an in silico study. *Europace*. 2018;20:iii26-iii35.
12. Pezzuto S, Quaglino A and Potse M. On Sampling Spatially-Correlated Random Fields for Complex Geometries. 2019:103-111.
13. Spach MS and Dolber PC. Relating extracellular potentials and their derivatives to anisotropic propagation at a microscopic level in human cardiac muscle. Evidence for electrical uncoupling of side-to-side fiber connections with increasing age. *Circ Res*. 1986;58:356-71.
14. Santangeli P and Marchlinski FE. Techniques for the provocation, localization, and ablation of non-pulmonary vein triggers for atrial fibrillation. *Heart Rhythm*. 2017;14:1087-1096.
15. Gharaviri A, Verheule S, Eckstein J, Potse M, Kuijpers NH and Schotten U. A computer model of endo-epicardial electrical dissociation and transmural conduction during atrial fibrillation. *Europace*. 2012;14 Suppl 5:v10-v16.

Table S1. Tissue conductivity parameters (σ) used in the simulations. The units are mS/cm. The subscript 'i' stands for intracellular, 'e' for extracellular, 'L' for longitudinal, 'T' for transverse (within a tissue sheet) and 'C' for across-sheet.

material	σ_{iL}	σ_{iT}	σ_{iC}	σ_{eL}	σ_{eT}	σ_{eC}	G_{mL}	G_{mT}	G_{mC}
wall	3.0	0.3	0.3	3.0	1.2	1.2	1.5	0.24	0.24
iso	1.5	1.5	1.5	1.5	1.5	1.5	0.75	0.75	0.75
BB	9.0	0.3	0.3	9.0	1.2	1.2	4.5	0.24	0.24
fibrotic	3.0	0.0	0.0	3.0	1.2	1.2	1.5	0	0

Table. S2 Atrial Fibrillation Cycle length **(**AFCL) in simulations with different ablation patterns (* P Value < 0.05).

Simulation groups / **Fibrosis**	**Control**	**PVI**	**BOX**	**PVI + LAAI**	**BOX + LAAI**
without	149±3.2ms	154± 2.3ms*	155± 2.7ms*	163± 2.4ms*	167± 2.7ms*
moderate	142± 3ms	149± 2ms*	153± 4.1ms*	157± 3ms*	158± 4.1ms*
severe	139± 2.4ms	146± 1.9ms	148 ± 3.4ms	151 ± 2.5ms*	152 ± 3.4ms*

Figure S1

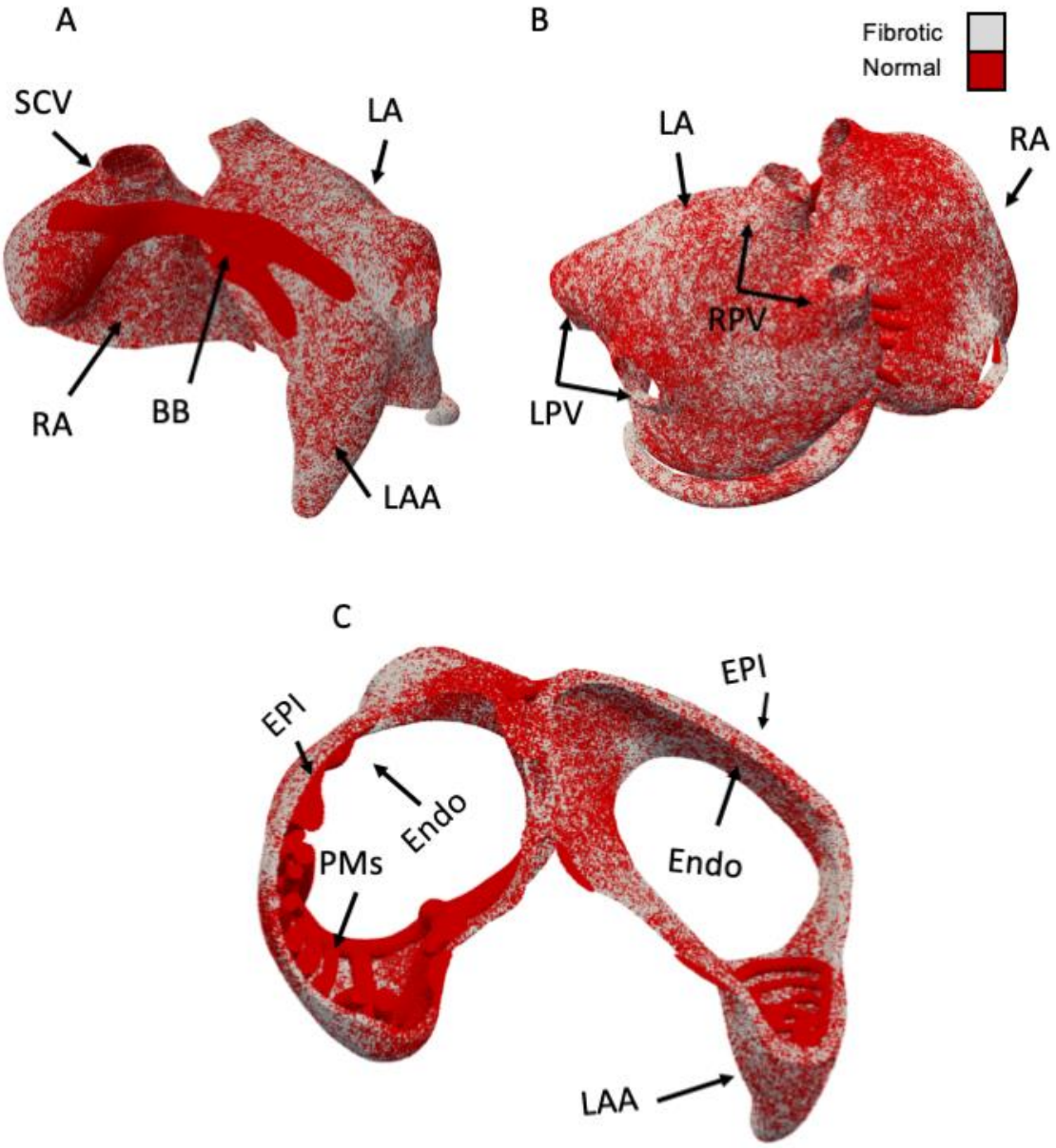
A
SCV
LA
RA
BB
LAA
B
Fibrotic
Normal
LA
RA
RPV
LPV
C
EPI
EPI
Endo
PMs
Endo
LAA

Figure S2

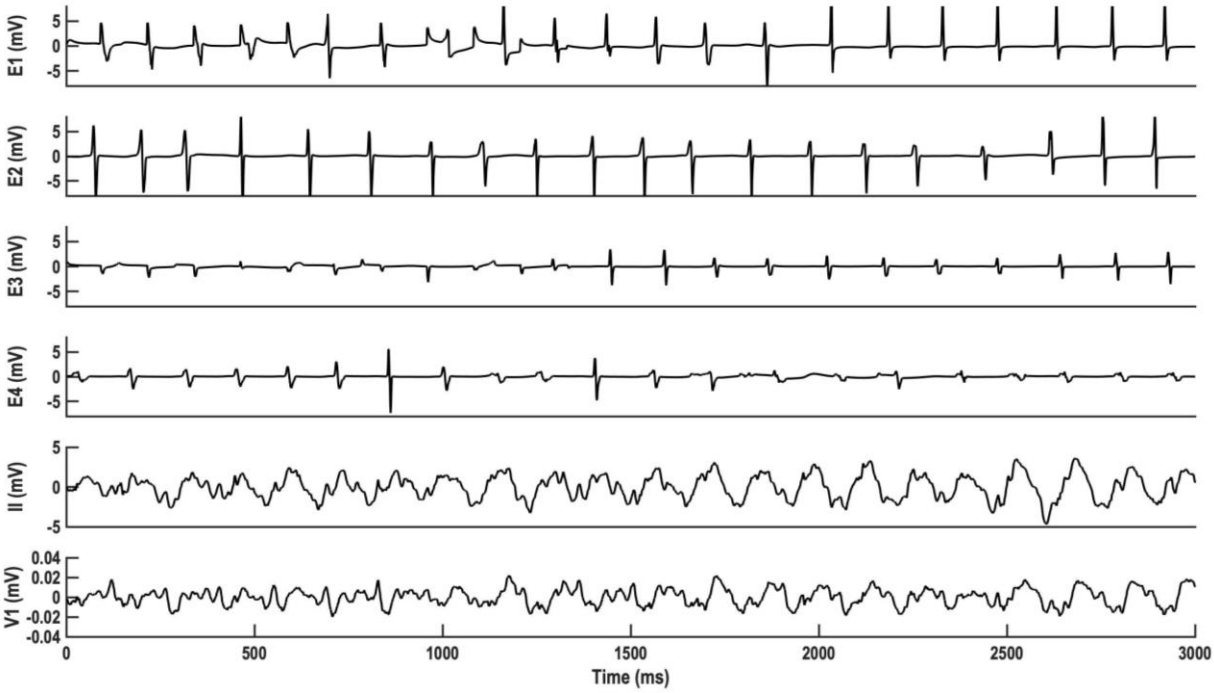
E1 (mV)
E2 (mV)
E3 (mV)
E4 (mV)
II (mV)
V1 (mV)
5
0
-5
0.04
0.02
-0.02
-0.04
0
500
1000
1500
2000
2500
3000
Time (ms)

Figure S3

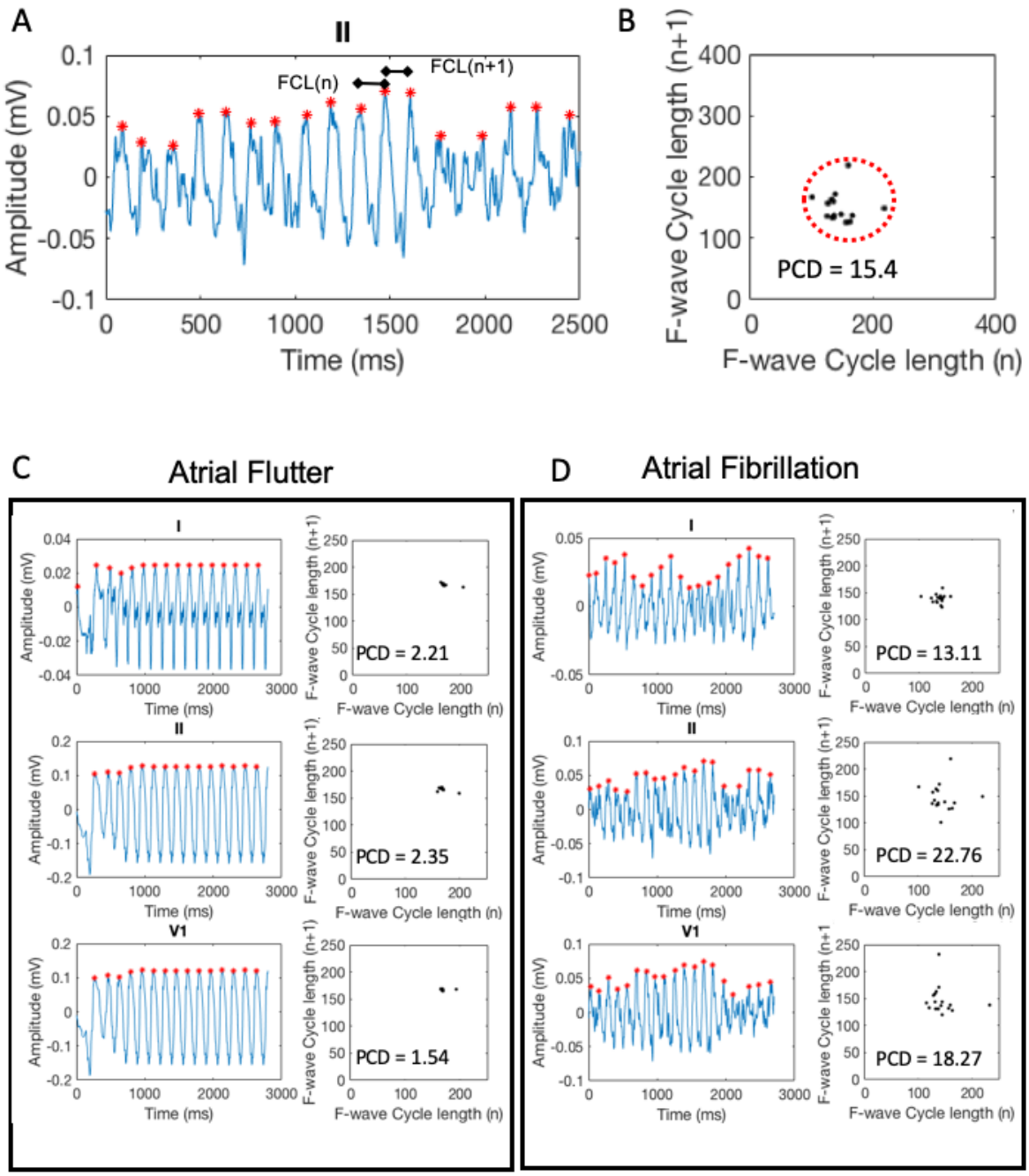
A
II
FCL(n)
FCL(n+1)
Amplitude (mV)
Time (ms)
B
F-wave Cycle length (n+1)
F-wave Cycle length (n)
PCD = 15.4
C
Atrial Flutter
D
Atrial Fibrillation
I
II
V1
PCD = 2.21
PCD = 2.35
PCD = 1.54
PCD = 13.11
PCD = 22.76
PCD = 18.27

Figure S4

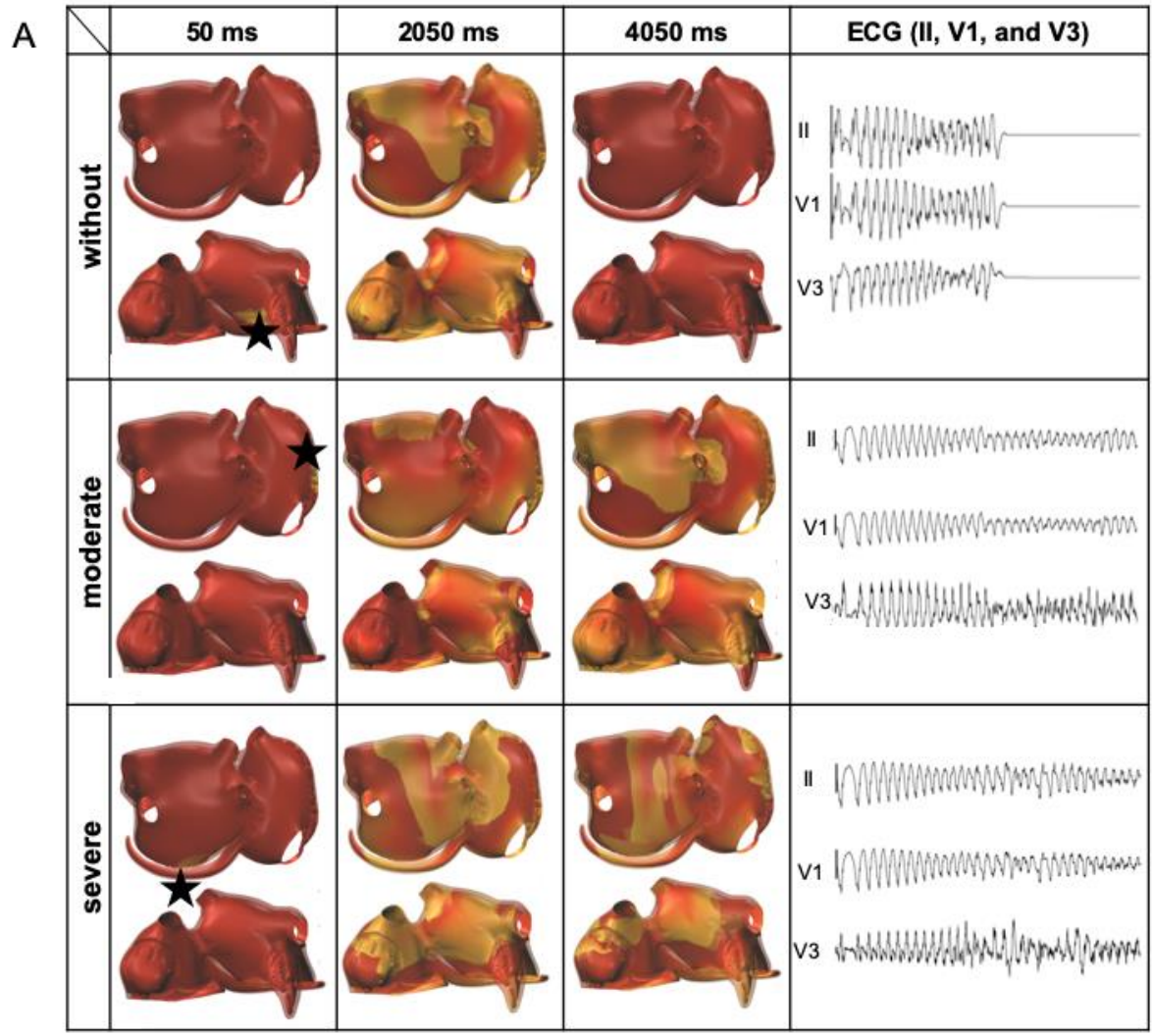
A
50 ms
2050 ms
4050 ms
ECG (II, V1, and V3)
without
moderate
severe
II
V1
V3

Figure S5